Insights of Electrical Engineering and Technology
https://ojs.achpub.com/IEET

Research Article

A Broadband Linearly Polarized Magneto-Electric Dipole Antenna with Microstrip Slot-Coupled Feed

Xinyi Li[1,2], Wusheng Ji[1,2,*], Jingbo Shi[1,2] and Haibo Li[1,2]

[1] Institute of Antenna and Microwave Techniques, Tianjin University of Technology and Education, Tianjin 300222, China
[2] School of Electronic Engineering, Tianjin University of Technology and Education, Tianjin 300222, China
E-mail: jiwusheng@tute.edu.cn

Received: 1 August 2025; **Revised:** 10 September 2025; **Accepted:** 29 September 2025

Abstract: This paper presents a broadband linearly polarized magneto-electric dipole antenna (MEDA) fed by a microstrip line through an aperture-coupled slot. This antenna abandons the traditional rectangular electric dipole patch and Γ-shaped probe feed; instead, the proposed design utilizes a trapezoidal electric dipole plate with arc-shaped slots and a vertical magnetic dipole plate to form the radiating structure. The antenna is excited by a microstrip feedline and a rectangular coupling aperture etched on the substrate. This feeding structure effectively improves the impedance matching and radiation characteristics, thereby significantly enhancing the overall antenna performance. Simulation results indicate that the antenna's impedance bandwidth ($|S_{11}|\leq$-10 dB) reaches 82.6% (2.89-6.96 GHz), with a maximum in-band gain of 9.49 dBi and a cross-polarization level below -30 dB.

Keywords: broadband; linear polarization; magneto-electric dipole; microstrip slot-coupled feed

1. Introduction

As a front-end core component of wireless communication systems, the performance of an antenna directly affects the system's transmission efficiency and operational reliability. With the rapid development of wireless communication technology, the demand for antennas with broad bandwidth and high gain has become increasingly prominent, forming a key focus of current research.

To meet the critical performance requirement for high gain in modern communication systems, microstrip patch antennas have been extensively studied. Utilizing a novel metamaterial region, reference [1] designed a microstrip high-gain bow-tie antenna for H-band applications, achieving a peak gain of 10.21 dBi at 7.5 GHz, demonstrating the potential of metamaterials for gain enhancement. By vertically embedding eight modified peacelogo planar metamaterials (MPLPM) and two two-sided MPLPMs (TSMPLPM) into the azimuth plane of a multiple-input multiple-output (MIMO) antenna, reference [2] achieved a return loss better than 10 dB over the 34.5-45.5 GHz frequency band and a peak gain of 15.5 dBi at 40 GHz, representing a significant improvement over the antenna structure without the metamaterial loading. Furthermore, reference [3] proposed a compact, high-gain, high-isolation wideband MIMO antenna, which achieved a peak gain of 17.1 dBi and an isolation of 36.7 dB through the use of a metamaterial superstrate and sidewall structures. However, such metamaterial antennas exhibit a relatively limited impedance bandwidth, making it difficult to simultaneously satisfy the performance requirements for both wide bandwidth and high gain.

Against this backdrop, magnetoelectric dipole antennas have demonstrated significant advantages. In 2006, based on the complementary principle, K. M. Luk first proposed the magnetoelectric dipole antenna [4], which achieved a 43.9% relative impedance bandwidth and possesses notable advantages such as wide impedance

DOI: https://doi.org/10.37256/xxxx

bandwidth, stable symmetric radiation patterns, and low cross-polarization, making it an ideal choice for new-generation communication systems. In recent years, scholars worldwide have conducted multifaceted research on magnetoelectric dipole antennas based on the complementary principle. Regarding low-profile design, references [5-7] significantly reduced the antenna's profile height and expanded its application scenarios by introducing folded vertical metal walls and improving the probe feeding structure. Reference [8] further proposed a compact wideband dual-polarized MEDA, which employs cross-differential feeding and integrates the radiating elements with the feeding network on a single metal layer, achieving a 39.4% impedance bandwidth from 26.3 to 39.1 GHz, effectively addressing the issues of narrow bandwidth and integration difficulties associated with traditional dual-polarized antennas in the millimeter-wave band. For bandwidth extension, reference [9] etched C-shaped slots on the surface of the electric dipole metal patch, increasing the antenna's impedance bandwidth to 55.4%; Reference [10] introduced a trapezoidal electric dipole structure and replaced the conventional probe feeding with microstrip line aperture-coupled feeding, further improving the antenna's bandwidth performance; Reference [11] embedded an improved feeding structure into the metal layer of the printed circuit board, achieving a low profile and good impedance matching. Furthermore, references [12,13] utilized the modes of dielectric resonators to equivalently function as magnetic and electric dipoles, effectively reducing the antenna size. To enhance antenna gain, reference [14] loaded a director above the magnetoelectric dipole antenna, increasing the maximum gain to 13.51 dBi; References [15-17] introduced parasitic elements to simultaneously optimize both bandwidth and gain performance. In terms of array design and MIMO applications, the magnetoelectric dipole antenna also demonstrates outstanding performance. Reference [18] designed a 4x4 magnetoelectric dipole antenna array excited by a microstrip line feeding network; this array achieved a 64.08% impedance bandwidth from 19.43 to 37.75 GHz, with a peak gain of up to 15.76 dBi. Reference [19] developed a four-port MIMO antenna based on a sequentially rotated circularly polarized array, achieving a 28.6% impedance bandwidth and a 21% axial ratio bandwidth, with a peak gain of 12.2 dBic, demonstrating promising application prospects in millimeter-wave communication systems. However, most antennas in the aforementioned studies feature complex structures, high fabrication difficulty, and elevated manufacturing costs, which limit their practical engineering applications.

To address the aforementioned issues, this paper undertakes multifaceted improvements and innovations based on the MEDA with microstrip line aperture-coupled feed proposed in reference [20]. In contrast to the rectangular electric dipole plate used in [20], this work employs a combined radiator structure comprising a modified trapezoidal plate and a rectangular plate with arc-shaped slots. This novel geometry achieves superior broadband performance and more stable radiation characteristics. Furthermore, the incorporation of a rectangular reflector cavity enhances the antenna gain. The main contributions of this work are summarized as follows:

1. A novel broadband linearly polarized MEDA is proposed, which utilizes a microstrip line aperture-coupled feed mechanism. This design abandons the traditional Γ-shaped probe feed and adopts a microstrip feedline printed on a dielectric substrate, excited through a rectangular coupling slot. Despite its relatively simple structure, the proposed antenna offers optimized impedance matching and radiation performance.
2. To improve impedance matching, a modified trapezoidal electric dipole plate with arc-shaped slots is introduced to replace the conventional rectangular dipole. This modification effectively excites multiple resonant modes, thereby broadening the impedance bandwidth, and also contributes to more stable gain and lower cross-polarization levels.
3. The use of the low-loss Rogers 6002 substrate reduces overall loss and improves antenna efficiency. In combination with the rectangular reflector cavity, this approach increases the overall gain by approximately 2 dBi, further enhancing the radiation performance.

2. Antenna Structure and Technical Description

As shown in Figure 1, the proposed broadband linearly polarized MEDA with microstrip slot-coupled feed consists of three components: a dielectric substrate, rectangular reflecting cavity, and magneto-electric dipole radiator. A square Rogers 6002 dielectric substrate with a dielectric constant of 2.94 and a loss tangent of 0.0012 was employed, with side length G_b and thickness T. The upper surface of the substrate serves as ground plane, containing a rectangular slot of length L_2 and width W_3 centered along the X-axis. The feeding microstrip line is attached to the substrate's bottom surface, extending from the edge to orthogonally intersect the slot, with length L_1 and width W_4. The rectangular reflecting cavity is fixed on the ground plane, constructed by four identical rectangular metal plates with length G_b and axial height G_h. The magneto-electric dipole radiator comprises two

identical radiating elements vertically placed on both sides of the ground plane's rectangular slot with symmetry, spaced by distance S_1. Each radiating element consists of a horizontally oriented trapezoidal metal plate and a vertically placed rectangular metal plate, where the trapezoidal plate has upper base W_2, lower base W_1, and height L, with an arc-shaped slot of width S_2 removed at distance L_3 from both ends of the lower base, dividing it into two sections, while the rectangular plate has height H and width W_2. The antenna's detailed dimensions are listed in Table 1.

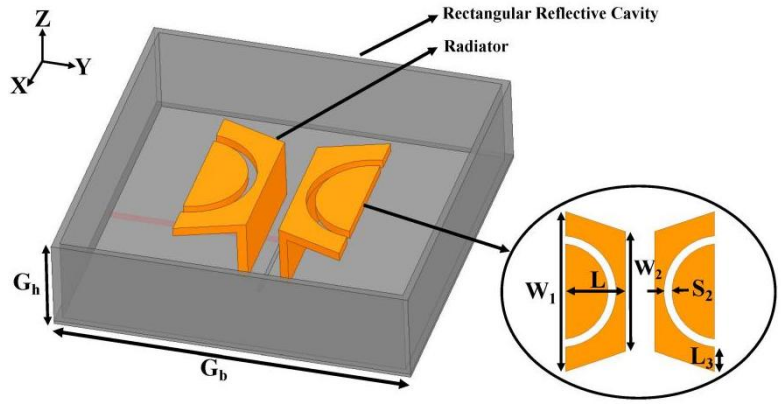

(a) Three-dimensional view of the antenna

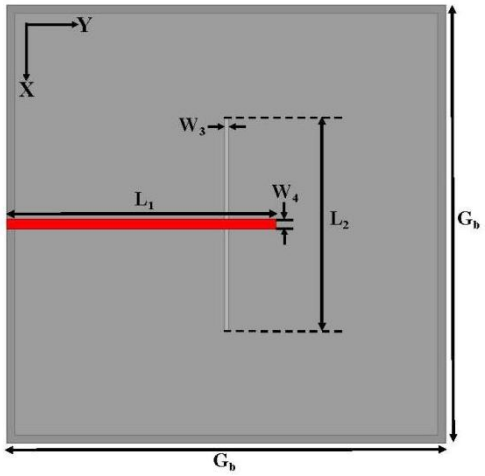

(b) Bottom view of the antenna

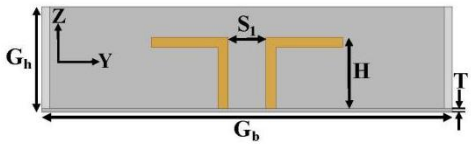

(c) Front view of the antenna

Figure 1. Schematic diagram of the antenna structure

Table 1. Antenna Dimension Parameters

Parameters	G_b	G_h	W_1	W_2	W_3	W_4	T
Value(mm)	80	20	40	34	0.8	1.8	0.762
Parameters	L	L_1	L_2	L_3	S_1	S_2	H
Value(mm)	15	49	39	6.065	3.65	2	14

3. Antenna Design Process

As clearly illustrated in Figure 2, the design evolution of the proposed antenna is demonstrated. The reflection coefficients and gain curves of three antenna prototypes are shown in Figure 3, where the left vertical axis indicates reflection coefficient (S_{11}) and the right axis represents antenna gain. Ant.1 is a MEDA configuration comprising two trapezoidal electric dipole plates and two vertical magnetic dipole plates, fed via microstrip aperture coupling, achieving 65.3% impedance bandwidth ($|S_{11}|\leq$-10 dB) from 3.51-6.91 GHz with peak in-band gain of 6.46 dBi. Ant.2 incorporates a rectangular reflecting cavity based on Ant.1's design, As evidenced by Fig. 3's curves, the added reflecting cavity enables, an enhanced 85.7% impedance bandwidth ($|S_{11}|\leq$-10 dB) spanning 2.78-6.95 GHz, with improved peak gain of 9.43 dBi. Ant.3 modifies Ant.2's radiator by introducing a 2 mm arc-shaped slot on the trapezoidal horizontal electric dipole, dividing it into two segments, achieving a final impedance bandwidth ($|S_{11}|\leq$-10 dB) of 82.6% (2.89-6.96 GHz) with peak in-band gain of 9.49 dBi. The reflection coefficient and gain curves in Fig. 3 demonstrate that this arc-slot introduction beneficially affects impedance matching, while ensuring stable bandwidth and gain performance across the operating spectrum.

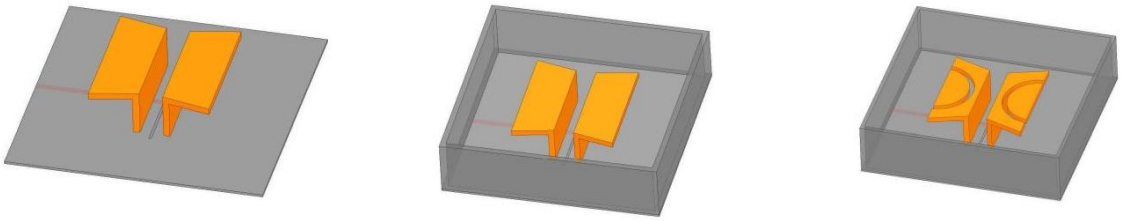

(a) Ant.1 (b) Ant.2 (c) Ant.3

Figure 2. Evolution of antenna design plot

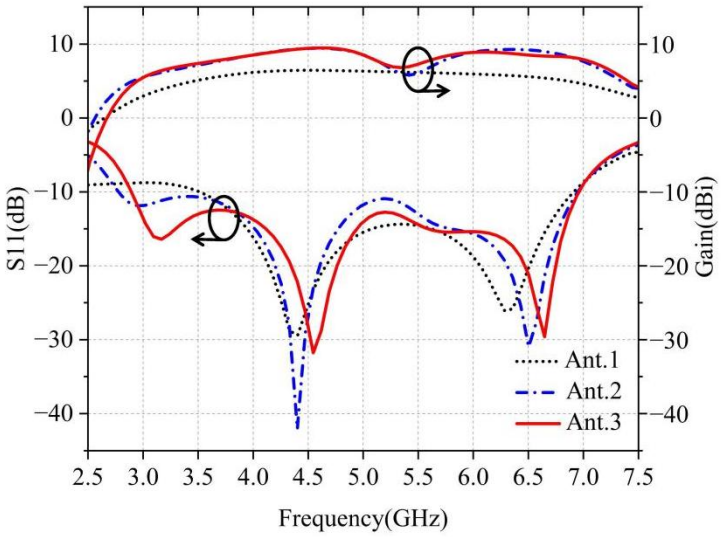

Figure 3. Comparison of S_{11} and Gain for Three Antennas

4. Working Principle of The Proposed Antenna

Figure 4 shows the equivalent circuit of the magnetic dipole and electric dipole [21]. In this circuit, an LC parallel circuit represents the magnetic dipole, while an LC series circuit represents the electric dipole. From the perspective of the entire circuit, the synergistic interaction between the magnetic and electric dipoles enables the antenna to achieve stable impedance matching over a broad frequency range, thereby contributing to excellent broadband and high-gain performance.

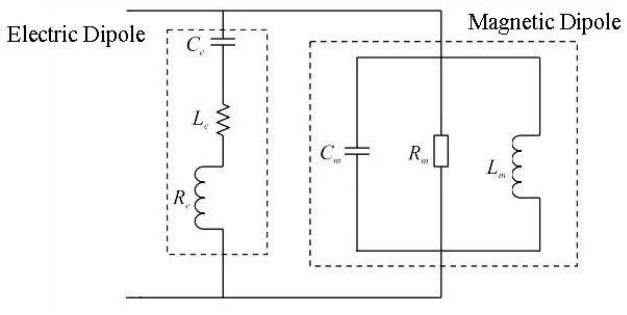

Figure 4. Equivalent circuit of the magnetoelectric dipole

Figure 5 illustrates the cavity magnetic dipole's electric field distribution and the radiator's equivalent current distribution. Fig. 5(a) demonstrates that the cavity's electric field primarily distributes along the y-axis direction. According to the equivalent current formula (1) in Reference [22]:

$$\overrightarrow{J_m}=-\hat{n}\times\vec{E} \tag{1}$$

The equivalent magnetic current density $\overrightarrow{J_m}$ of the open cavity is derived as shown in Figure 5b. Figure 5b reveals that the magnetic current components along the z-axis exhibit opposite phases and equal amplitudes, resulting in canceled radiation fields. When the cavity width S_1 is smaller than the free-space wavelength λ_0 (where λ_0 corresponds to the center frequency), the cavity behaves as an equivalent magnetic current source. The conduction current $\vec{J_e}$ on the horizontal metal plate forms an equivalent electric dipole, making this radiator a magneto-electric dipole structure.

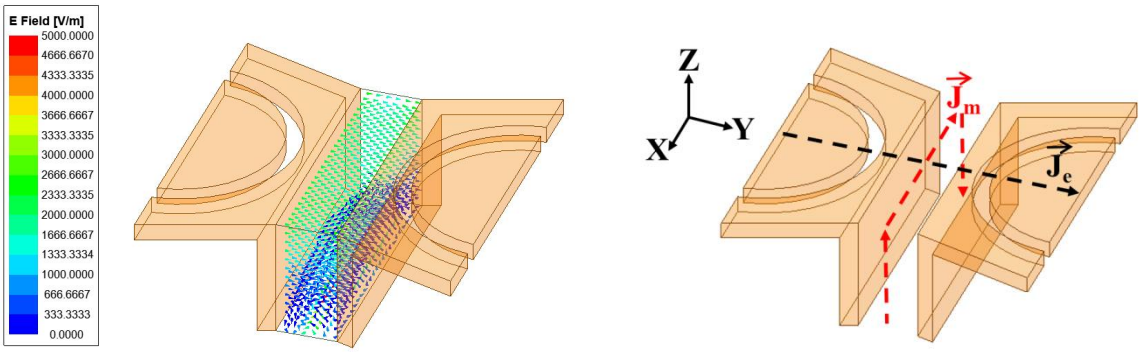

(a) Cavity Magnetic Dipole Electric Field Distribution (b) Radiator Equivalent Current Distribution

Figure 5. Cavity Magnetic Dipole Electric Field Distribution and Radiator Equivalent Current Distribution

At 4.9 GHz, the current distribution on the antenna radiator at different time instants within one period is shown in Figure 6. At t=0, the horizontal current on the horizontal metal plate of the magnetoelectric dipole radiator is predominantly in the -y direction, while the current on the vertical rectangular metal plate is weak, indicating that the electric dipole mode is excited at this moment. At t=T/4, the surface current on the horizontal metal plate of the magnetoelectric dipole radiator is weakest, while the currents on the two vertical metal plates dominate and flow in opposite directions. These currents, together with the ground plane they are attached to, form current loops equivalent to magnetic dipoles, thereby exciting the magnetic dipole mode. At t=T/2, the electric dipole mode is excited again, with the current direction mainly along the +y direction, opposite to the direction at t=0. At t=3T/4, the magnetic dipole mode is excited again, with the current direction opposite to that at t=T/4. This demonstrates that the magnetoelectric dipole radiator achieves radiation through the alternating operation of both electric and magnetic dipole modes.

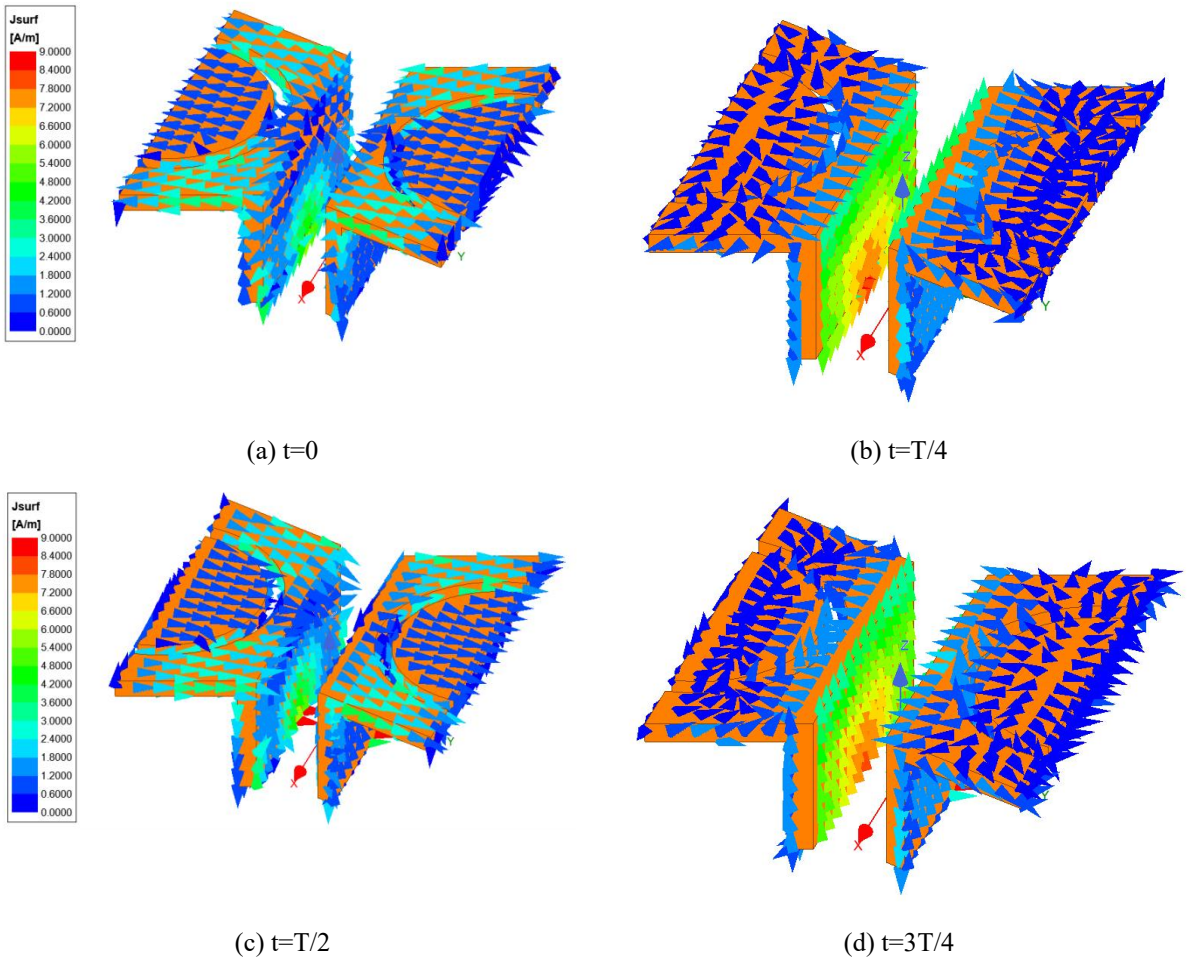

Figure 6. Current distribution of the proposed antenna at different time instants within one cycle at 4.9 GHz

5. Key Parameter Study of The Antenna

To more clearly understand the antenna's operational states under parameter variations, parametric scanning and analysis were conducted using the electromagnetic simulation software HFSS, by adjusting these critical parameters, their impacts on antenna performance can be better understood.

G_h represents the height of the rectangular reflecting cavity, and its impact on antenna performance is shown in Figure 7. The return loss curves demonstrate a low-frequency shifting trend as G_h increases, though its influence on impedance bandwidth remains limited. Simultaneously, both low and high frequency return loss curves elevate with larger G_h, ultimately causing the low-frequency reflection coefficient to exceed -10 dB, indicating impedance mismatch. Therefore, G_h=20 mm is selected to achieve optimal impedance matching.

W_2 denotes the upper base length of the trapezoidal electric dipole plate, and Figure 8 illustrates its impact on antenna performance. As shown, increasing W_2 shifts the low-frequency portion of return loss curves toward higher frequencies while moving the high-frequency portion toward lower frequencies, resulting in gradual reduction of the impedance bandwidth. At W_2=34 mm, the antenna achieves optimal impedance bandwidth coverage across the entire frequency range. Therefore, W_2=34 mm is selected to maximize the impedance bandwidth.

S_2 is the width of the arc-shaped slot removed from the trapezoidal electric dipole plate, and Figure 9 demonstrates its impact on antenna performance. As shown, the antenna's return loss curves exhibit a trend of shifting toward higher frequencies with increasing S_2. At S_2=2 mm, the antenna achieves relatively wide impedance bandwidth and excellent impedance matching across the entire band. Therefore, S_2=2 mm is selected based on comprehensive impedance matching evaluation.

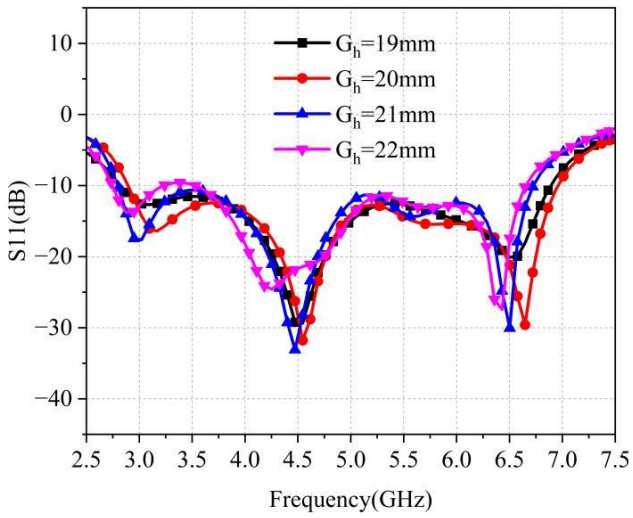

Figure 7. Effect of G_h Variation on Antenna Performance

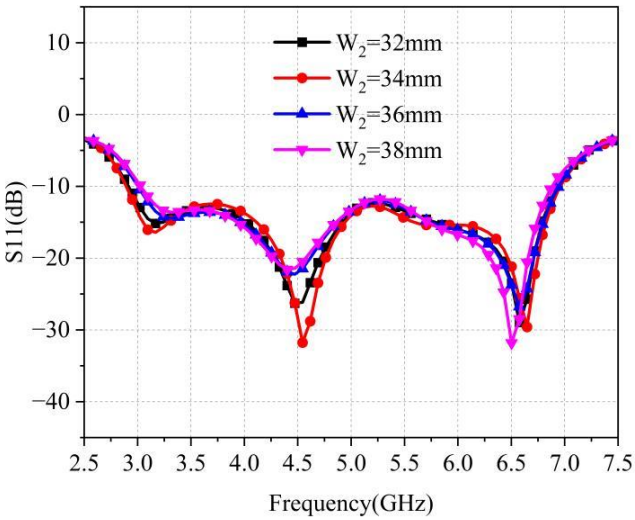

Figure 8. Effect of W_2 Variation on Antenna Performance

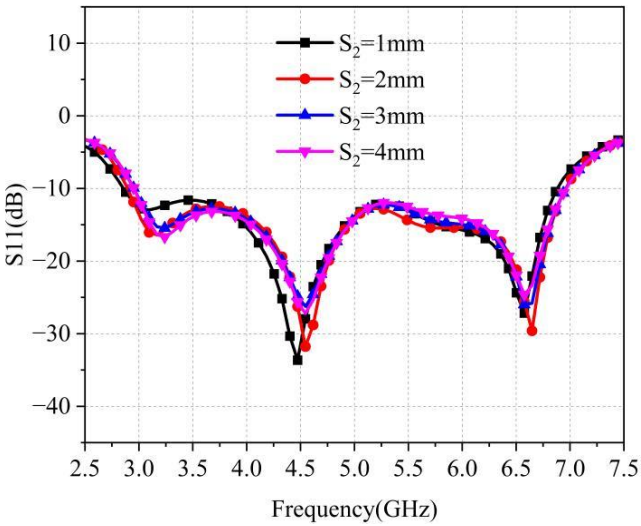

Figure 9. Effect of S_2 Variation on Antenna Performance

6. Antenna Simulation Results

Figure 10 shows the simulated reflection coefficient and gain curves of the proposed antenna. To comprehensively evaluate the antenna performance, this study employed two full-wave simulation software, HFSS and CST, for collaborative verification and comparison. Regarding impedance bandwidth, the HFSS simulation yielded an antenna impedance bandwidth ($|S_{11}|$≤-10 dB) of 82.6% (2.89 -6.96 GHz), while the CST results showed an antenna impedance bandwidth ($|S_{11}|$≤-10 dB) of 80.8% (2.93-6.90 GHz). A minor discrepancy exists between the two in terms of impedance bandwidth, primarily stemming from differences in discretization strategies and boundary condition handling between the Finite Element Method (FEM) and the Finite Integration Technique (FIT) for broadband simulations, yet they still demonstrate good consistency. Regarding gain performance, both software simulations yielded an in-band maximum gain of 9.49 dBi, indicating highly consistent predictions of radiation characteristics and further validating the effectiveness of the simulation models. Collectively, the simulation data from HFSS and CST mutually support each other, indicating the reliability of the antenna's broadband performance and radiation characteristics.

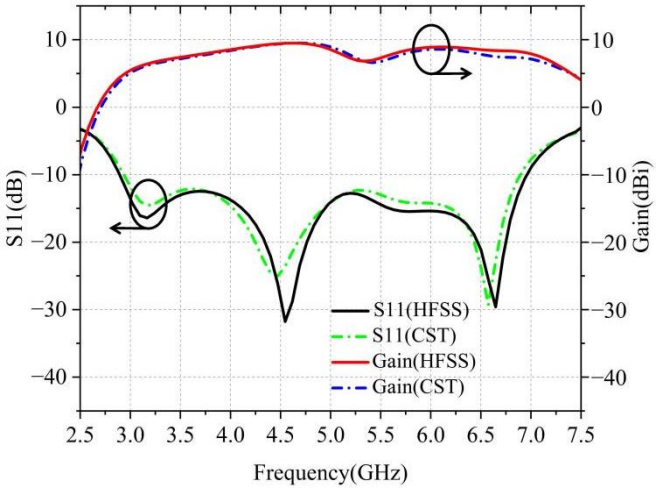

Figure 10. Simulated reflection coefficient and gain curves

The radiation patterns at 3.9 GHz, 4.9 GHz and 5.9 GHz are presented in Figure 11. The E-plane and H-plane radiation patterns exhibit excellent symmetry across the entire operating band, such symmetry being a crucial figure-of-merit for magneto-electric dipole antenna designs, demonstrating stable radiation performance at different frequencies. On the E-plane, the cross-polarization level at 4.9 GHz is below -35 dB, indicating excellent cross-polarization suppression. H-plane cross-polarization remains below -30 dB across the band, reaching under -40 dB at 4.9 GHz, demonstrating minimal cross-polarization that effectively reduces interference and enhances signal quality.

The performance comparison between the antenna proposed in this paper and published MEDAs is shown in Table 2. Based on the traditional magnetoelectric dipole, reference [23] reduced the antenna height and altered the current path by folding the radiating arms, while changing the feeding method to a metal-embedded PCB structure. This design achieved a cross-polarization level of 40 dB, but its impedance bandwidth was only 45% (1.7-2.7 GHz) with a maximum gain of 7.87 dBi, both lower than the performance of the antenna proposed in this paper. Reference [24] increased the maximum gain to 13.51 dBi by loading a magnetoelectric dipole director above the MEDA, however its impedance bandwidth ($|S_{11}|$≤-10 dB) was only 29.21% (1.90-2.55 GHz), while also increasing the antenna profile height, limiting practical application scenarios. Reference [25] reduced the antenna's profile height by designing the horizontal patch into an E-shape and folding the vertical shorting patch, achieving a 66.7% impedance bandwidth and 8.6 dBi peak gain, but both its bandwidth and gain performance are lower than the antenna scheme proposed in this paper. Reference [26] employed a novel ridged waveguide aperture-coupled feeding technique to excite the MEDA, achieving a 104% ultra-wideband impedance bandwidth, but the antenna structure is relatively complex, difficult to fabricate, and has low gain, making it hard to meet the high-gain requirements of modern communication systems. Reference [27] constructed a 4×4 MEDA array using a three-layer segmented patch (SEP) structure and excited it

through a microstrip line feed network, achieving a peak gain of 18.2 dBic. However, the impedance bandwidth of this array antenna is only 36.1%, and it suffers from high cross-polarization issues. The comparison results indicate that the antenna proposed in this paper can balance both impedance bandwidth and gain-two key antenna performance metrics-while also offering the advantage of low cross-polarization, making it better suited to meet the requirements of modern communication systems.

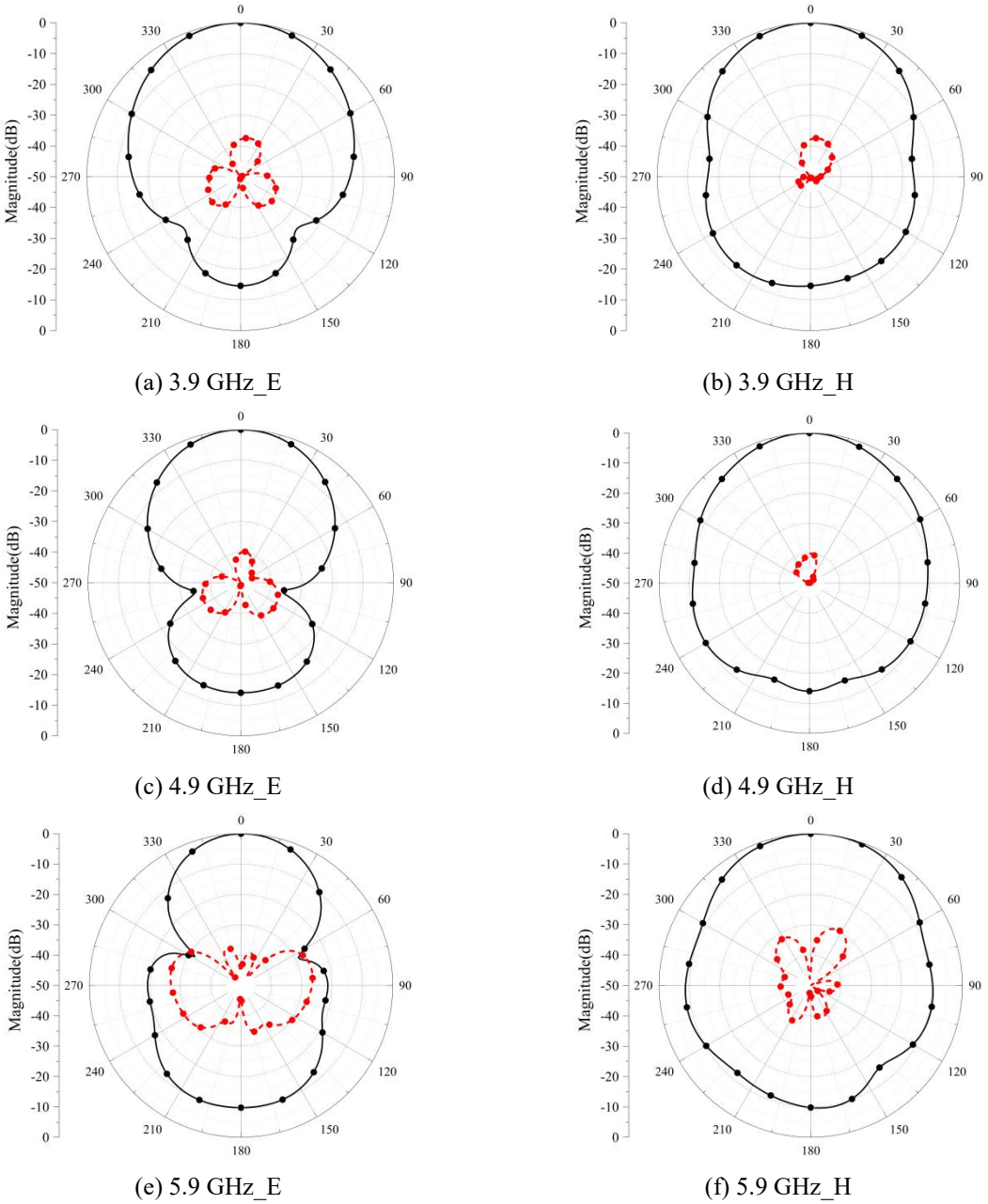

(a) 3.9 GHz_E (b) 3.9 GHz_H

(c) 4.9 GHz_E (d) 4.9 GHz_H

(e) 5.9 GHz_E (f) 5.9 GHz_H

Figure 11. Simulated radiation patterns of the antenna at 3.9 GHz, 4.9 GHz, and 5.9 GHz, including both co-polarization and cross-polarization components

Table 2. The Antenna Proposed is Compared to Other Antennas

Ref.	Imp. BW(%)	Imp. BW(GHz)	Size	Maximum Gain	Cross-pol
[23]	45	1.7-2.7	0.46 λ_0 × 0.3 λ_0 × 0.057 λ_0	7.87 dBi	40 dB
[24]	29.21	1.9-2.55	1.748 λ_0 × 1.748 λ_0 × 0.775 λ_0	13.51 dBi	25 dB
[25]	66.7	1.8-3.6	\	8.9 dBi	28 dB
[26]	104	1.99-6.14	1.12 λ_0 × 1.12 λ_0 ×0.76 λ_0	7.5 dBi	20 dB
[27]	29.7	29.15-42.0	3.2 λ_0 × 3.2 λ_0 × 0.22 λ_0	18.2 dBic	15 dB
Prop.	82.6	2.89-6.96	1.31 λ_0 × 1.31 λ_0 ×0.33 λ_0	9.49 dBi	30 dB

7. Conclusion

This paper proposes a broadband linearly polarized MEDA fed by microstrip line aperture coupling. Compared with traditional linearly polarized MEDAs, this antenna uses a trapezoidal electric dipole metal plate with arc-shaped defects and a vertically placed magnetic dipole metal plate to form the radiator, and employs microstrip line aperture coupling for feeding, demonstrating good integration characteristics. Simulation results show that the proposed antenna achieves an impedance bandwidth ($|S_{11}|$≤-10 dB) of 82.6% (2.89-6.96 GHz), a peak gain of 9.49 dBi, and a cross-polarization level below -30 dB. Furthermore, the antenna features a simple structure and flexible design, showing high application potential in sub-6GHz band communication systems.

Author Contributions

Simulation, computation and writing, X.L.; Review and revision, W.J.; Technical support, J.S. and H.L.

Funding

This work is supported by Tianjin Key Projects of Research and Development and Science and Technology Support in 2020 (20YFZCGX00700), and Tianjin Enterprise Science and Technology Commissioner Project in 2022 (22YDTPJC00330).

Acknowledgments

The authors express their reciprocal appreciations for efficient collaborations.

Conflict of Interest

There is no conflict of interest for this study.

References

[1] F. Khajeh-Khalili, M. A. Honarvar, M. Naser-Moghadasi, et al., "A simple method to enhance gain and isolation of MIMO antennas simultaneously based on metamaterial structures for millimeter-wave applications," *J. Infrared, Millimeter, Terahertz Waves*, vol. 42, no. 11, pp. 1078-1093, 2021. DOI:10.1007/s10762-021-00834-2.

[2] F. Khajeh-Khalili, M. A. Honarvar, M. Naser-Moghadasi, et al., "Gain enhancement and mutual coupling reduction of multiple-input multiple-output antenna for millimeter-wave applications using two types of novel metamaterial structures," *Int. J. RF Microw. Comput.-Aided Eng.*, vol. 30, no. 1, p. e22006, 2020. DOI: 10.1002/mmce.22006.

[3] F. Khajeh-Khalili, M. A. Honarvar, M. Naser-Moghadasi, et al., "High-gain, high-isolation, and wideband millimetre-wave closely spaced multiple-input multiple-output antenna with metamaterial wall and metamaterial superstrate for 5G applications," *IET Microw. Antennas Propag.*, vol. 15, no. 4, pp. 379-388, 2021. DOI: 10.1049/mia2.12055.

[4] K. M. Luk and H. Wong, "A new wideband unidirectional antenna element," *Int. J. Microw. Opt. Technol.*, vol. 1, no. 1, pp. 35-44, 2006.

[5] X. Huang, W. Cao, and L. Lu, "A Ultra-Wideband Magneto-Electric Dipole Antenna With Improved Feeding Structure," in 2024 Int. Appl. Comput. Electromagn. Soc. Symp. (ACES-China), 2024, pp. 1-3. DOI: 10.1109/ACES-China62474.2024.10699579

[6] Y. Liu, M. Li, Y. Zhang, et al., "Compact magneto-electric dipole antenna with low-profile for LTE femtocell base stations," in 2016 Asia-Pacific Conf. Antennas Propag. (APCAP), 2017, pp. 1-3. DOI: 10.1109/APCAP.2017.8420315

[7] L. Ge, S. Gao, D. Zhang, et al., "Magnetoelectric dipole antenna with low profile," *IEEE Antennas Wireless Propag. Lett.*, vol. 17, no. 10, pp. 1760-1763, 2018. DOI: 10.1109/LAWP.2018.2866064.

[8] Y. Yang, B. Feng, X. Ding, et al., "A Low-profile Broadband Dual-polarized Magneto-electric Dipole Antenna for 5G Applications," in *2025 8th World Conf. Comput. Commun. Technol. (WCCCT)*, 2025, pp. 251-254. DOI: 10.1109/WCCCT65447.2025.11027925.

[9] G. Zhang, L. Ge, J. Wang, et al., "Design of a 3-D integrated wideband filtering magneto-electric dipole antenna," *IEEE Access*, vol. 7, pp. 4735-4740, 2018. DOI: 10.1109/ACCESS.2018.2882817.

[10] F. Shang, X. Yan, and Z. Fu, "A broadband electromagnetic dipole antenna with microstrip line gap coupling feeding," in 2023 IEEE 11th Asia-Pacific Conf. Antennas Propag. (APCAP), 2023, pp. 1-2. DOI: 10.1109/APCAP59480.2023.10470000.

[11] Y. Chen, F. C. Zeng, and Z. Y. Zhang, "A Low-Profile Folded Magnetoelectric Dipole Antenna for Mobile Communication," *IEEE Antennas Wireless Propag. Lett.*, 2025. DOI: 10.1109/LAWP.2025.3527565.

[12] S. Zheng and X. Chen, "A Compact Broadband Dielectric Resonator Magnetoelectric Dipole Antenna," in 2023 Int. Appl. Comput. Electromagn. Soc. Symp. (ACES-China), 2023, pp. 1-3. DOI: 10.23919/ACES-China60289.2023.10249828.

[13] S. Song and X. Chen, "A compact and broadband dielectric resonator magnetoelectric dipole antenna with high front-to-back ratio," *IEEE Antennas Wireless Propag. Lett.*, vol. 23, no. 1, pp. 239-243, 2023. DOI: 10.1109/LAWP.2023.3322276.

[14] L. Y. Feng and C. Q. Zhang, "Compact magneto-electric dipole director loaded high-gain dual-polarized magneto-electric dipole antenna," *IEEE Antennas Wireless Propag. Lett.*, vol. 23, no. 7, pp. 2130-2134, 2024. DOI: 10.1109/LAWP.2024.3382879.

[15] B. Zhou, T. Wu, Z. Y. Zhang, et al., "A wideband dual-polarization magneto-electric dipole antenna with low-profile and high-gain," in 2023 IEEE 11th Asia-Pacific Conf. Antennas Propag. (APCAP), 2023, pp. 1-2. DOI: 10.1109/APCAP59480.2023.10470201.

[16] M. Behboudi, J. Nourinia, and C. Ghobadi, "Miniaturized printed X-band magneto-electric dipole antenna by loading parasitic elements," in *2024 11th Int. Symp. Telecommun. (IST)*, 2024, pp. 561-566. DOI: 10.1109/IST64061.2024.10843516.

[17] G. H. Sun, K. Wang, and L. W. Qin, "Design of a dual-polarized magnetoelectric dipole with gain enhancement based on patch loading," *IEEE Trans. Antennas Propag.*, 2024. DOI: 10.1109/TAP.2024.3496080.

[18] X. Zhao, J. Sheng, Z. Wang, et al., "A Wideband Magneto-Electric Dipole Antenna Array for Millimeter-Wave Applications," in 2023 IEEE 11th Asia-Pacific Conf. Antennas Propag. (APCAP), 2023, pp. 1-2. DOI: 10.1109/APCAP59480.2023.10469768.

[19] P. Ghosh, A. Gorai, S. Behera, et al., "A Compact MIMO Array Antenna with Wideband Circular Polarization Using Magneto-Electric Dipole Elements for Millimeter-Wave Applications," *J. Infrared, Millimeter, Terahertz Waves*, vol. 46, no. 3, p. 24, 2025. DOI: 10.1007/s10762-025-01035-x.

[20] X. Cui, F. Yang, M. Gao, et al., "A wideband magnetoelectric dipole antenna with microstrip line aperture-coupled excitation," *IEEE Trans. Antennas Propag.*, vol. 65, no. 12, pp. 7350-7354, 2017. DOI: 10.1109/TAP.2017.2762007.

[21] K. M. Luk and B. Wu, "The magnetoelectric dipole—A wideband antenna for base stations in mobile communications," *Proc. IEEE*, vol. 100, no. 7, pp. 2297-2307, 2012.DOI: 10.1109/JPROC.2012.2187039.

[22] L. Sun, Y. Hou, Y. Li, et al., "An open cavity leaky-wave antenna with vertical-polarization endfire radiation," *IEEE Trans. Antennas Propag.*, vol. 67, no. 5, pp. 3455-3460, 2019. DOI: 10.1109/TAP.2019.2902662.

[23] Y. Chen, F. C. Zeng, and Z. Y. Zhang, "A Low-Profile Folded Magnetoelectric Dipole Antenna for Mobile Communication," *IEEE Antennas Wireless Propag. Lett.*, 2025. DOI: 10.1109/LAWP.2025.3527565.

[24] C. Q. Zhang and L. Y. Feng, "Design of high-gain magneto-electric dipole antenna by loading a magneto-electric dipole director," *IEEE Antennas Wireless Propag. Lett.*, vol. 22, no. 8, pp. 1823-1827, 2023. DOI: 10.1109/LAWP.2023.3266263.

[25] H. Cheng, B. Yuan, X. H. Zhang, et al., "Wideband E-shaped magneto-electric dipole antenna," in *2016 IEEE Int. Conf. Microw. Millimeter Wave Technol. (ICMMT)*, 2016, vol. 2, pp. 638-640. DOI: 10.1109/ICMMT.2016.7762393.

[26] Q. Chen, F. Cui, and B. Zhang, "A 3-D printed ultrawideband magnetoelectric dipole antenna with ridged waveguide aperture-coupled feeding," *IEEE Antennas Wireless Propag. Lett.*, vol. 22, no. 4, pp. 814-818, 2022. DOI: 10.1109/LAWP.2022.3225862.

[27] Z. Wang and Z. H. Tu, "Wideband circularly polarized antenna array using three-layer segmented patches for Q-band application," *IEEE Antennas Wireless Propag. Lett.*, vol. 22, no. 9, pp. 2055-2059, 2022. DOI: 10.1109/LAWP.2022.3200046.